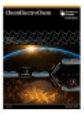

Stable and Active Oxygen Reduction Catalysts with Reduced Noble Metal Loadings through Potential Triggered Support Passivation

Daniel Göhl,*[a] Holger Rueß,[b] Stefanie Schlicht,[c] Alexandra Vogel,[a] Michael Rohwerder,[a] Karl J. J. Mayrhofer,[d, e] Julien Bachmann,[c, f] Yuriy Román-Leshkov,[g] Jochen M. Schneider,[b] and Marc Ledendecker*[a, h]

The development of stable, cost-efficient and active materials is one of the main challenges in catalysis. The utilization of platinum in the electroreduction of oxygen is a salient example where the development of new material combinations has led to a drastic increase in specific activity compared to bare platinum. These material classes comprise nanostructured thin films, platinum alloys, shape-controlled nanostructures and core–shell architectures. Excessive platinum substitution, however, leads to structural and catalytic instabilities. Herein, we introduce a catalyst concept that comprises the use of an atomically thin platinum film deposited on a potential-triggered passivating support. The model catalyst exhibits an equal specific activity with higher atom utilization compared to bulk platinum. By using potential-triggered passivation of titanium carbide, irregularities in the Pt film heal out via the formation of insoluble oxide species at the solid/liquid interface. The adaptation of the described catalyst design to the nanoscale and to high-surface-area structures highlight the potential for stable, passivating catalyst systems for various electrocatalytic reactions such as the oxygen reduction reaction.

1. Introduction

The understanding of fundamental catalytic processes on an atomic level has led to drastic improvements in activity and stability for various industrially relevant reactions. The oxygen reduction reaction (ORR) is a salient example where new material concepts have led to drastic improvements in activity. Nanostructured thin films[1], surface de-alloyed or shape-controlled nanoparticles[2,3] have shown their potential by increasing the surface area normalized specific (SA) and mass normalized activity (MA) at lower, associated costs. While platinum (Pt) is the element with the highest specific activity towards the ORR, its scarcity is its major disadvantage.[4] An interesting, yet not industrially established concept comprises the use of core-shell structures with a cost-efficient core material that supports a noble metal film with a thickness lying in the monolayer (ML) range.[5–9] The main advantages of such a design over monometallic catalysts are enhanced SA,[10,11] a drastic decrease in noble metal loading and significant cost benefits.[12] Critically for these materials, the main challenge lies in the stability of the non-noble material that supports the noble metal layer.[13–16] State-of-the-art Pt-based alloys and intermetallic phases with 3d transition metals (TM) such as Pt_3Ni, Pt_3Co or Pt_3Cu equally develop a core-shell structure during operation until a closed Pt-film protects the particle interior from dissolution. Given that non-protected, non-noble alloy elements such as Ni, Co or Cu dissolve quantitatively under fuel cell operating conditions,[17–19] noble metal contents of up to 80 at% are often employed.[2,20,21] Metal leaching results in extensive losses in the overall catalytic activity and poisoning of the proton conducting membrane, constraining the broad usage of core-shell structures with earth abundant elements.[16]

[a] D. Göhl, A. Vogel, Dr. M. Rohwerder, Dr. M. Ledendecker
Department of Interface Chemistry and Surface Engineering
Max-Planck-Institut für Eisenforschung GmbH
40237 Düsseldorf, Germany
E-mail: d.goehl@mpie.de
[b] Dr. H. Rueß, Prof. Dr. J. M. Schneider
Materials Chemistry, RWTH Aachen University
52074 Aachen, Germany
[c] Dr. S. Schlicht, Prof. Dr. J. Bachmann
Department of Chemistry and Pharmacy
Friedrich-Alexander University Erlangen-Nürnberg
91058 Erlangen, Germany
[d] Prof. Dr. K. J. J. Mayrhofer
Helmholtz-Institute Erlangen-Nürnberg for Renewable Energy
Forschungszentrum Jülich GmbH
91058 Erlangen, Germany
[e] Prof. Dr. K. J. J. Mayrhofer
Department of Chemical and Biological Engineering
Friedrich-Alexander-Universität Erlangen-Nürnberg
91058 Erlangen, Germany
[f] Prof. Dr. J. Bachmann
Institute of Chemistry
Saint Petersburg State University
Saint Petersburg 198504, Russian Federation
[g] Prof. Dr. Y. Román-Leshkov
Department of Chemical Engineering
Massachusetts Institute of Technology
Cambridge, MA 02139, USA
[h] Dr. M. Ledendecker
Department of Technical Chemistry
Technical University Darmstadt
64287 Darmstadt, Germany
E-mail: marc.ledendecker@tu-darmstadt.de

Supporting information for this article is available on the WWW under https://doi.org/10.1002/celc.202000278

New material combinations are ardently needed to reduce the total noble metal content and suppress non-noble element dissolution while keeping the specific and mass activity high. In this manuscript, we introduce a catalyst concept that comprises the use of a potential-triggered, passivating support material and a few monolayer thick, supported Pt-film. The feasibility of the proposed design is exemplified over a range of model thin film compositions subjected to *in-* and *ex-situ* characterization methods. Specifically, flow cell (FC) measurements were coupled to an inductively coupled mass spectrometer (ICP-MS) to measure *operando* metal dissolution as a function of applied potential. Together with scanning Kelvin probe force microscopic (SKPFM) scans and X-ray photoelectron spectroscopy (XPS), a detailed topographic and surface potential map was compiled and correlated to the elemental surface composition and dissolution trajectories. The proposed catalyst design offers increased Pt-utilization through controlled noble metal deposition ranging from sub-monolayer to multilayer coverages. The concept of potential triggered passivation is exemplarily introduced for titanium carbide (TiC) as support material where superior catalytic stability was achieved at SAs comparable to state-of-the-art Pt_3NiMo octahedra.

2. Results and Discussion

In a previous study, imperfect Pt coverages on a non-noble core material has led to fast and quantitative dissolution of the core revealing the need for material combinations that can withstand the harsh ORR conditions.[22] Early transition metal carbides were reported to exhibit metallic conductivity, high corrosion resistance and are able to strongly bind to noble metals such as Pt anchoring it in place.[7,8,23] Our own research revealed stabilization of tungsten carbide compared to bare tungsten,[24] and we were able to identify the metal-carbon bond enthalpy as stabilization criterion for various metal carbides.[25] Titanium carbide (TiC) shows a maximum formation and bonding enthalpy compared to other transition metal carbides resulting in enhanced thermodynamic stabilization.[25] We used exemplarily readily available TiC and deposited multiple Pt-layers on a 510 nm thick magnetron sputtered TiC thin film via atomic layer deposition (ALD) offering high control over the final metal film.[26–28] Comprehensive characterization of the support, as well as detailed descriptions of the TiC preparation conditions and the ALD process can be found in the SI (Figure S1, S2, S3, Table S1). The Pt films comprise thicknesses ranging from 1 to 6 monolayers.[26,29–31] We used the Pt_{xML}/TiC nomenclature where *X* indicates the number of deposited Pt-monolayers. The SA and MA towards the ORR were determined via thin-film rotating disk electrode (TF-RDE) measurement at 1,600 rpm in O_2-saturated 0.1 M $HClO_4$ applying the Koutecky-Levich's equation. The electrochemical surface area (ECSA) was determined via CO stripping and hydrogen underpotential deposition.[32] The values of both methods were averaged for determining the specific activity. (c.f. Experimental section in the SI, Table S2, Figure S4).[33,34] The use of film electrodes required the use of a special RDE set-up that allows for activity measurements of catalyst films deposited on non-conductive substrates.[35] The SA and MA at 0.95 V_{RHE} for Pt-layer thicknesses of 3 and 6 monolayers are shown in Figure 1. Pt_{3ML}/TiC displayed a surprisingly low ORR activity of 0.034 ± 0.012 mA cm$^{-2}_{Pt}$ which originates from stability problems arising from low Pt surface coverage (*vide infra*).[36] The SA of Pt_{6ML}/TiC (0.27 ± 0.06 mA cm$^{-2}_{Pt}$ at 0.95 V_{RHE}, Figure 1) exceeds the activity of high surface area, commercially available 3 nm Pt nanoparticles supported on Vulcan (Pt_{3nm}/C, 0.09 ± 0.01 mA cm$^{-2}_{Pt}$) by a factor of three. The SA is slightly higher than state-of-the-art Pt_3NiMo octahedra supported on hollow graphitic spheres (0.24 ± 0.02 mA cm$^{-2}_{Pt}$) and competes with bulk Pt (0.26 ± 0.02 mA cm$^{-2}_{Pt}$, Figure S5).[37] The enhanced SA can be correlated to a weakened oxygen binding energy that goes along with a downshift of the d-band center as visualized by a shifted CO oxidation peak potential (Table S2).[9,38] Our results support interpretations from Arenz and coworkers who found that low interparticle edge-to-edge distances result in electric double layer overlap which was attributed to the observed increased SA.[39] It is likely that the deposited Pt-film mimics bulk Pt and that potential electronic/geometric effects from TiC are shielded by the six platinum monolayers. In contrast to bulk Pt, the enhanced noble metal utilization through thin film structuring leads to a MA of 0.054 ± 0.001 A g$^{-1}_{Pt}$ which is comparable to Pt-nanoparticles supported on a high surface area carbon support(Pt_{3nm}/C) (0.060 ± 0.014 A g$^{-1}_{Pt}$).[37]

After establishing the general applicability of Pt/TiC as ORR catalysts, its dissolution behavior was investigated in a flow cell (FC) by recording a cyclic voltammogram (CV) at 3 mV s^{-1} between 0.0 and 1.5 V_{RHE} (Figure 2a, Figure S6). The FC was coupled to an inductively coupled plasma mass spectrometer (ICP-MS) that allows for *operando* monitoring of potential- and time- resolved metal dissolution in the ppb range.[24,41] For both elements, the dissolution is strongly dependent on the film morphology and thickness. Below 1.5 monolayers of deposited platinum, TiC oxidizes at potentials above 1.0 V_{RHE}. At the same time, the total Ti dissolution decreases from 1 dissolved monolayer (ML_{Diss}) (bare TiC, for calculation details see SI) to 0.5

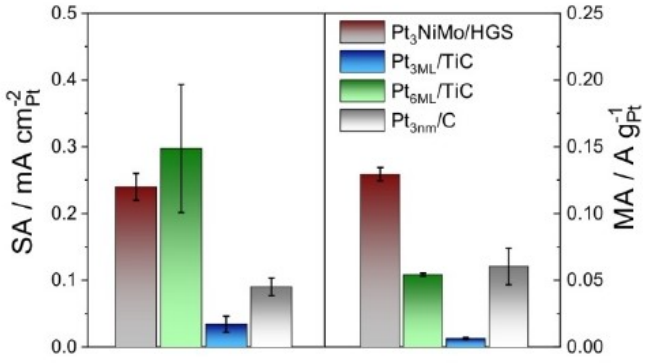

Figure 1. Oxygen reduction specific (left) and mass (right) activities of Pt_{6ML}/TiC (4.6 μg_{Pt} cm^{-2}) and Pt_{3ML}/TiC (1.3 μg_{Pt} cm^{-2}).[40] The activity was determined from the Koutecky-Levich equation by subtracting the Ar background from iR-corrected ORR polarization curves at 0.95 V_{RHE} in O_2-saturated 0.1 M $HClO_4$ at 50 mV s^{-1} and 1600 rpm. As reference samples, 3 nm Pt nanoparticles supported on carbon (TKK, 46 wt% Pt) and Pt_3NiMo octahedra supported on hollow graphitic spheres (15 wt% Pt) were used.

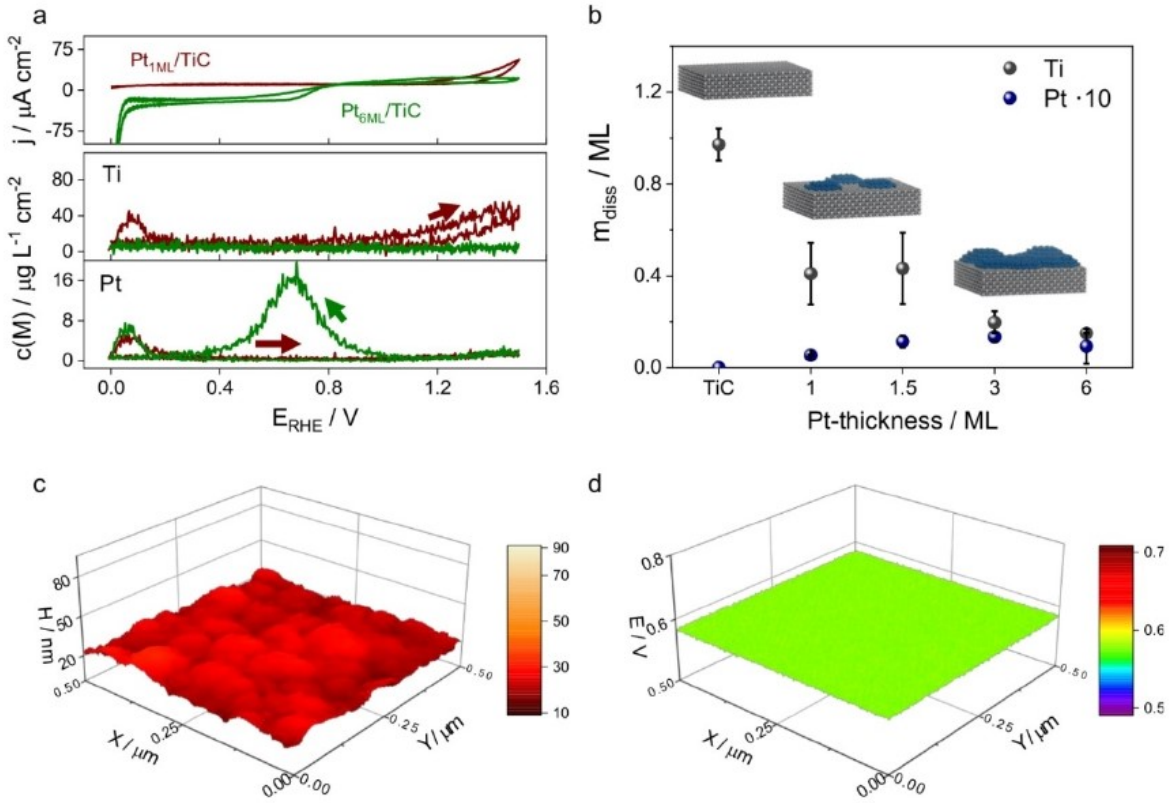

Figure 2. a) Cyclic voltammograms and the corresponding Ti and Pt dissolution profiles of Pt_{1ML}/TiC and Pt_{6ML}/TiC from 0.0 to 1.5 V_{RHE} in 0.1 M $HClO_4$ at 3 mV s^{-1}. b) The corresponding total dissolved amount of Ti and Pt in monolayers for all samples. c) Topographic and d) potential scanning Kelvin probe force microscopic scans of Pt_{6ML}/TiC.

ML_{Diss} ($Pt_{1.5ML}$/TiC, Figure 2b, 3a). For Pt thicknesses over 1.5 monolayers, Ti dissolution drops further and occurs concomitantly to Pt transient dissolution. The dissolved Pt amount goes hand in hand with the increased amount of deposited Pt up to Pt_{3ML}/TiC. When augmenting the layer thickness further, an improved stability and a lower Pt dissolution rate was observed for Pt_{6ML}/TiC compared to Pt_{3ML}/TiC. We assigned the higher stability to a lower amount of dissolution prone defect and edge sites, which is also confirmed by scanning Kelvin probe force microscopy (SKP-FM) measurements.[42] Heavily utilized in the field of corrosion, SKP-FM offers access to surface morphologies and electrochemical properties and thereby indirectly to the surface composition.[43,44] By measuring the surface potential with spatial resolution of up to a few nanometers, Pt covered areas can be distinguished from oxidized, exposed TiC (Figure S3).[45,46] Together with topographic scans, an exact image of surface composition and morphology is obtained. The topographic scan of Pt_{6ML}/TiC reveals disk-shaped Pt particles (Figure 2c) which is in line with the small dependency of the Pt signal on the incident beam angle observed in angle-dependent XPS measurements (Figure S7). Both results are in agreement with minor increase in root-mean-squared (RMS) surface roughness from 1.6 nm for TiC to 2.4 nm for Pt_{6ML}/TiC (Figure S8a). The potential scan mode revealed negligible potential differences for Pt_{6ML}/TiC (Figure 2d) and strongly supports a closed packing of Pt to cover the TiC surface through a nearly continuous Pt-film. The surface potentials of bare Pt and TiC can be found in Figure S8b. In contrast, $Pt_{1.5ML}$/TiC shows clear surface potential differences along the Pt grain boundaries with a higher fraction of surface exposed TiC (Figure S8c,d) and a higher surface roughness. For Pt_{6ML}/TiC, the continuous Pt-film enhances the stability and improves the SA drastically compared to lower Pt thicknesses.

Besides the aim for homogeneity and a continuous Pt film, the support properties are crucial for the performance of the whole catalytic system. To illustrate the superior stability of a self-healing transition metal carbide compared to other non-noble materials, bare TiC was cycled from - 0.2 to 1.5 V_{RHE} at 3 mV s^{-1} in 0.1 M $HClO_4$ (Figure 3a) in the FC/ICP-MS system. TiC oxidation starts at potentials higher than 0.85 V_{RHE} concomitant with detectable Ti dissolution. According to thermodynamics, soluble TiO^{2+} species are formed upon oxidation [Eq. (1)]:[47]

$$TiC + 3H_2O \rightarrow TiO^{2+} + CO_2 + 8e^- + 6H^+ \quad (1)$$

When the potential is further raised, the oxidation current reaches a maximum at 1.2 V_{RHE}. This leads to a local oversaturation of TiO^{2+} near the electrode surface and the formation of insoluble $TiO_2 \cdot H_2O$ [Eq. (2)]:[47,48]

$$TiO^{2+} + 2H_2O \rightarrow TiO_2 \cdot H_2O + 2H^+ \quad (2)$$

When the potential is further ramped up, current and dissolution concentrations decline as the ratio of passivating,

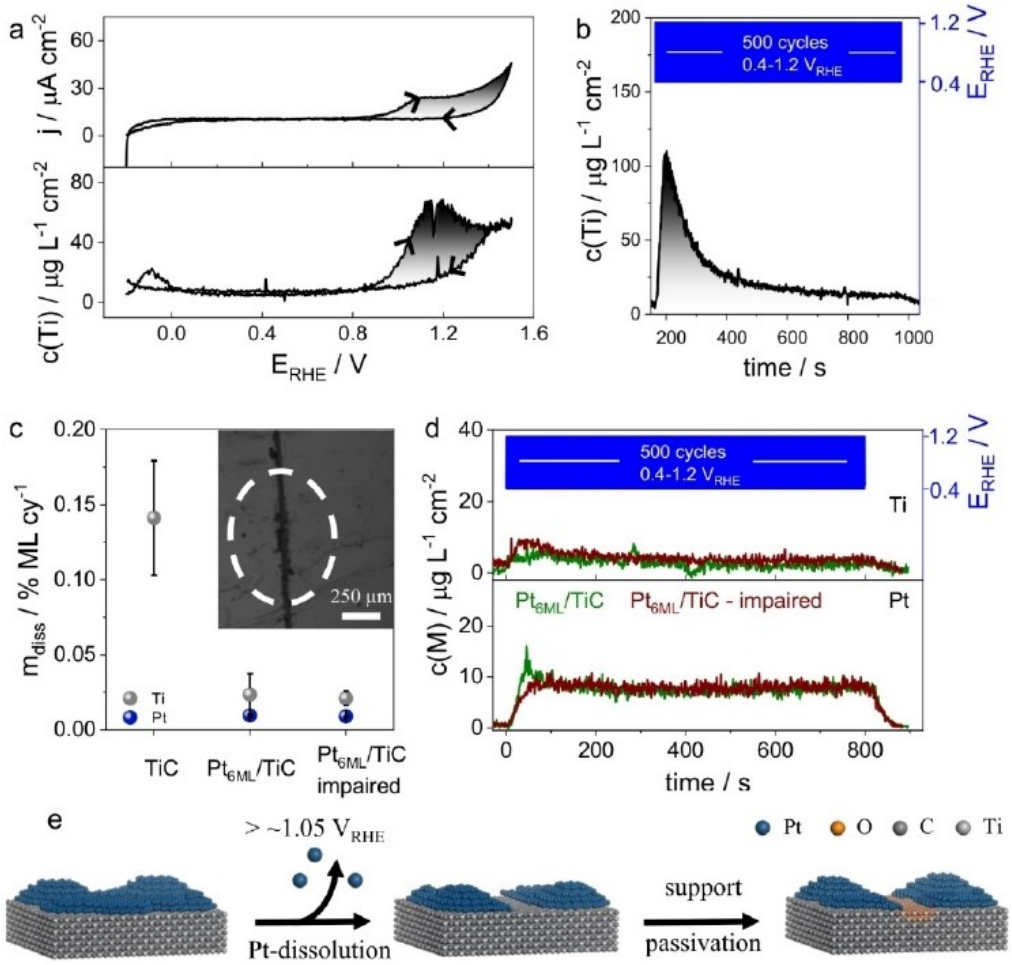

Figure 3. a) Cyclic voltammogram and the corresponding Ti dissolution profiles of bare TiC from - 0.2 to 1.5 V_{RHE} at 3 mV s^{-1} in 0.1 M $HClO_4$. b) Ti dissolution profile during 500 cycles between 0.4 and an upper potential limit of 1.2 V_{RHE} at 1 V s^{-1} in 0.1 M $HClO_4$. c) Total dissolved amounts of Ti and Pt for experiments (b) and (d). The inset displays the image of the damaged surface of Pt_{6ML}/TiC and the electrochemically measured area (white dotted line). d) Ti and Pt dissolution profile during 500 cycles between 0.4 and 1.2 V_{RHE} at 1 V s^{-1} in 0.1 M $HClO_4$. The corresponding current-voltage diagrams for (b) and (d) can be found in Figures S7 and S8. e) Schematic showing the concept of potential-triggered support passivation to stabilize the platinum film.

solid TiO_2 to soluble TiO^{2+} species increases. At these potentials, the surface passivates efficiently and stops further dissolution (A detailed discussion about the passivation mechanism can be found in the SI, Schematic S1). On a nobility scale according to the value of the dissolution equilibrium potential, TiC exhibits a higher practical nobility than classical coinage metals such as Ni, Co or Fe.[47] As shown before in our group, these metals are not stable at these potentials and dissolve nearly quantitatively. The same holds true for other carbides (WC), sulfides (MoS_2) and phosphides (Ni_5P_4, Co_2P) that dissolve at open circuit potential and do not passivate efficiently in acidic medium.[19]

At 1.2 V_{RHE}, where passivation starts to prevail, the potential is slightly higher than the oxidation potential of Pt/PtO_x as reported by Topalov et. al., who gave a value of 1.05 V_{RHE} under the conditions used in the present work. Since Pt does not dissolve at potentials below 1.05 V_{RHE}, a continuous Pt overlayer protects TiC from dissolution.[49] To illustrate the protection of the transition metal carbide by Pt against oxidation and dissolution at lower potentials, we applied 500 load cycles between 0.4 and 1.0 V_{RHE} at 1 V s^{-1} to Pt_{6ML}/TiC and Pt_{3ML}/TiC. The total amount of dissolved Ti declines from 0.22% of a monolayer per cycle (ML·cy^{-1}) for pure TiC (Figures S9a and S10) to 0.01% ML·cy^{-1} for Pt_{3ML}/TiC and is with 0.005% ML·cy^{-1} almost undetectable for Pt_{6ML}/TiC (Figure S10, S11a). The higher degradation of not fully covered Pt_{3ML}/TiC explains the previously described low ORR activity and emphasizes the need for homogeneous noble metal coverages. That the high stability of Pt_{6ML}/TiC originates from the degree of surface coverage and not from the intrinsic stability increase of the 6 ML thick Pt film itself compared to a 3 ML thick film, is supported by comparing the dissolution of sputtered and ALD deposited 5–6 ML thick Pt films on TiWC (Figure S12).

However, despite full coverages and preferential binding between TiC and Pt,[50] potential excursions over 1.05 V lead to platinum oxidation and transient Pt dissolution which creates imperfections in the covering Pt layer. In agreement with the passivation observed for pristine TiC (Figure 3a), the underlying and exposed support surface passivates at higher potentials, which minimizes dissolution and stabilizes the system. The proposed concept of potential-triggered support passivation is

displayed in Figure 3e. To test our hypothesis and to gain additional insights into the passivation properties of the Pt/TiC system, bare TiC was cycled 500 times between 0.4 and 1.2 V_{RHE} and the potential-dependent dissolution was monitored *in-situ* (Figure 3b,c). The dissolution of bare TiC was compared to fully covered and surface impaired (≈5% of total surface area) Pt_{6ML}/TiC (Figure 3c,d). The Faradaic dissolution efficiency of bare TiC declines to around 40% (Figure S9b, for calculation details see SI), resulting in a small dissolution rate of 0.05% ML·cy^{-1} after the 500th potential cycle. The measured overall dissolution rate is four times lower compared to 500 potential cycles between 0.4 and 1.0 V_{RHE} and is as important as the observed low dissolution efficiency. Compared to that, both the deliberately damaged and pristine samples show similar dissolution profiles with further declined total dissolved amounts of about 0.022% and 0.009% ML·cy^{-1} for Ti and Pt, respectively. Accelerated dissolution of TiC was not observed for the impaired surface, demonstrating the efficient passivation as incomplete surface passivation would have led to an expected increase in Ti dissolution by more than 40% (c.f. SI, eq. S8). The superior stability of TiC becomes evident when it is compared to non-passivating TMCs such as WC and VC which are covered by 6 ML of Pt. Here, substantial dissolution of the underlying substrate occurs once the protecting Pt film is oxidized (Figure S13). Additionally to the stability, the ORR specific and mass activity of the impaired Pt_{6ML}/TiC sample remained high and is comparable to as-prepared Pt_{6ML}/TiC demonstrating the general feasibility of the proposed catalyst concept (Figure S5), which can be adapted to a wide range of electrocatalytic reactions where high oxidative potentials and low pH values are needed.

3. Conclusions

Our results outline a new strategy to increase Pt-utilization through potential-triggered passivation of the underlying support to increase the catalytic potential of platinum. To secure high stability and activity during operation, the deposition of a closed Pt film protects the non-noble metal from dissolution at potentials below 1.05 V_{RHE}. At higher potentials where Pt oxidation and dissolution occur, the underlying TiC heals out the defects and imperfections created in the Pt film by building a protective oxide layer that stops further degradation. These results highlight the possibilities for tailored materials with synergistic behavior between noble metal film and non-noble support for enhanced stability. Our approach of optimized platinum utilization could be extended to other potential-triggered, strong passivating supports and core materials with reduced passivation potentials. Adapting the described catalyst design to the nanoscale and to high-surface-area structures has the potential to keep a high specific activity and further increase the noble metal utilization, while maintaining a high stability.

Experimental Section

A detailed description of the experimental details can be found in the Supporting Information.

Acknowledgements

D.G. and K.J.J.M. want to thank the Federal Ministry for Economic Affairs and Energy (BMWi) of Germany in the framework of PtTM@HGS (project number 03ET6080 A) for funding. M.L. acknowledge the Federal Ministry of Education and Research (BMBF) in the framework of NanoMatFutur (SynKat) for financial support (project number 03XP0265). Further, S.S. and J.B. acknowledge the German Ministry of Education and research (BMBF) in the project 'Tubulair±' (project number 03SF0436G) and the German Research Foundation (DFG) via the Excellence Cluster "Engineering of Advanced Materials" (EXC315) for funding. H.R. and J.M.S. gratefully acknowledges financial support from the MPG fellow program. Y.R.-L. acknowledges the Toyota Research Institute through the Accelerated Materials Design and Discovery program.

Conflict of Interest

The authors declare no conflict of interest.

Keywords: electrocatalysis · fuel cells · nanostructures · oxygen reduction reaction · self-healing

[1] D. Van Der Vliet, C. Wang, M. Debe, R. Atanasoski, N. M. Markovic, V. R. Stamenkovic, *Electrochim. Acta* **2011**, *56*, 8695–8699.
[2] P. Strasser, S. Koh, T. Anniyev, J. Greeley, K. More, C. Yu, Z. Liu, S. Kaya, D. Nordlund, H. Ogasawara, M. F. Toney, A. Nilsson, *Nat. Chem.* **2010**, *2*, 454–460.
[3] C. Cui, L. Gan, H. Li, S. Yu, M. Heggen, P. Strasser, *Nano Lett.* **2012**, *12*, 5885–5889.
[4] O. Gröger, H. A. Gasteiger, J.-P. Suchsland, *J. Electrochem. Soc.* **2015**, *162*, A2605–A2622.
[5] A. L. Strickler, A. Jackson, T. F. Jaramillo, *ACS Energy Lett.* **2016**, *2*, 244–249.
[6] J. X. Wang, H. Inada, L. Wu, Y. Zhu, Y. Choi, P. Liu, W. P. Zhou, R. R. Adzic, *J. Am. Chem. Soc.* **2009**, *131*, 17298–17302.
[7] X. Tian, H. Tang, J. Luo, H. Nan, T. Shu, L. Du, J. Zeng, S. Liao, R. R. Adzic, *ACS Catal.* **2017**, *7*, 3810–3817.
[8] S. T. Hunt, M. Milina, A. C. Alba-Rubio, C. H. Hendon, J. A. Dumesic, Y. Román-Leshkov, *Science* **2016**, *352*, 974–978.
[9] A. Garg, M. Milina, M. Ball, D. Zanchet, S. T. Hunt, J. A. Dumesic, Y. Román-Leshkov, *Angew. Chem. Int. Ed.* **2017**, *56*, 8828–8833; *Angew. Chem.* **2017**, *129*, 8954–8959.
[10] E. Fako, A. S. Dobrota, I. A. Pašti, N. López, S. V. Mentus, N. V. Skorodumova, *Phys. Chem. Chem. Phys.* **2018**, *20*, 1524–1530.
[11] P. Liu, J. K. Nørskov, *Phys. Chem. Chem. Phys.* **2001**, *3*, 3814–3818.
[12] M. Ledendecker, S. Geiger, K. Hengge, J. Lim, S. Cherevko, A. M. Mingers, D. Göhl, G. V. Fortunato, D. Jalalpoor, F. Schüth, C. Scheu, K. J. J. Mayrhofer, *Nano Res.* **2019**, *12*.
[13] S. T. Hunt, T. M. Kokumai, D. Zanchet, Y. Román-Leshkov, *J. Phys. Chem. C* **2015**, *119*, 13691–13699.
[14] C. H. Hendon, S. T. Hunt, M. Milina, K. T. Butler, A. Walsh, Y. Román-Leshkov, *J. Phys. Chem. Lett.* **2016**, *7*, 4475–4482.

[15] D. V. Esposito, S. T. Hunt, A. L. Stottlemyer, K. D. Dobson, B. E. McCandless, R. W. Birkmire, J. G. Chen, *Angew. Chem. Int. Ed.* **2010**, *49*, 9859–9862; *Angew. Chem.* **2010**, *122*, 10055–10058.
[16] H. Shan, W. Gao, Y. Xiong, F. Shi, Y. Yan, Y. Ma, W. Shang, P. Tao, C. Song, T. Deng, H. Zhang, D. Yang, X. Pan, J. Wu, *Nat. Commun.* **2018**, *9*, 1011.
[17] J. Knossalla, P. Paciok, D. Göhl, D. Jalalpoor, E. Pizzutilo, A. M. Mingers, M. Heggen, R. E. Dunin-Borkowski, K. J. J. Mayrhofer, F. Schüth, M. Ledendecker, *J. Am. Chem. Soc.* **2018**, *140*, 15684–15689.
[18] A. K. Schuppert, A. Savan, A. Ludwig, K. J. J. Mayrhofer, *Electrochim. Acta* **2014**, *144*, 332–340.
[19] M. Ledendecker, J. S. Mondschein, O. Kasian, S. Geiger, D. Göhl, M. Schalenbach, A. R. Zeradjanin, S. Cherevko, R. E. Schaak, K. Mayrhofer, *Angew. Chem. Int. Ed.* **2017**, *56*, 9767–9771; *Angew. Chem.* **2017**, *129*, 9899–9903.
[20] F. J. Lai, W. N. Su, L. S. Sarma, D. G. Liu, C. A. Hsieh, J. F. Lee, B. J. Hwang, *Chem. Eur. J.* **2010**, *16*, 4602–4611.
[21] M. Oezaslan, P. Strasser, *J. Power Sources* **2011**, *196*, 5240–5249.
[22] D. Göhl, A. Garg, P. Paciok, K. J. J. Mayrhofer, M. Heggen, Y. Shao-Horn, R. E. Dunin-Borkowski, Y. Román-Leshkov, M. Ledendecker, *Nat. Mater.* **2019**.
[23] S. T. Hunt, M. Milina, Z. Wang, Y. Roman-Leshkov, *Energy Environ. Sci.* **2016**, 3290–3301.
[24] D. Göhl, A. M. Mingers, S. Geiger, M. Schalenbach, S. Cherevko, J. Knossalla, D. Jalalpoor, F. Schüth, K. J. J. Mayrhofer, M. Ledendecker, *Electrochim. Acta* **2018**, *270*, 70–76.
[25] D. Göhl, H. Rueß, M. Pander, A. R. Zeradjanin, K. J. J. Mayrhofer, J. M. Schneider, A. Erbe, M. Ledendecker, *J. Electrochem. Soc.* **2020**, *167*, 21501.
[26] R. W. Johnson, A. Hultqvist, S. F. Bent, *Mater. Today* **2014**, *17*, 236–246.
[27] D. V. Esposito, J. G. Chen, *Energy Environ. Sci.* **2011**, *4*, 3900–3912.
[28] R. Schlitz, A. A. Amusan, M. Lammel, S. Schlicht, T. Tynell, J. Bachmann, G. Woltersdorf, K. Nielsch, S. T. B. Goennenwein, A. Thomas, *Appl. Phys. Lett.* **2018**, *112*, 242403.
[29] S. Schlicht, M. K. S. Barr, M. Wu, P. Hoppe, E. Spiecker, W. Peukert, J. Bachmann, *ChemElectroChem* **2018**, *5*, 3932–3937.
[30] A. Jablonski, J. Zemek, *Surf. Interface Anal.* **2009**, *41*, 193–204.
[31] C. J. Powell, A. Jablonski, *NIST Electron Inelastic-Mean-Free-Path Database, SRD 71*, National Institute Of Standards And Technology, Gaithersburg MD, **2010**.
[32] K. J. J. Mayrhofer, D. Strmcnik, B. B. Blizanac, V. Stamenkovic, M. Arenz, N. M. Markovic, *Electrochim. Acta* **2008**, *53*, 3181–3188.
[33] D. F. Van Der Vliet, C. Wang, D. Li, A. P. Paulikas, J. Greeley, R. B. Rankin, D. Strmcnik, D. Tripkovic, N. M. Markovic, V. R. Stamenkovic, *Angew. Chem. Int. Ed.* **2012**, *51*, 3139–3142; *Angew. Chem.* **2012**, *124*, 3193–3196.
[34] D. V. Malevich, V. B. Drozdovich, I. M. Zharskii, *Stud. Surf. Sci. Catal.* **1997**, *112*, 359–366.
[35] M. D. Pohl, S. Haschke, D. Göhl, O. Kasian, J. Bachmann, K. J. J. Mayrhofer, I. Katsounaros, *J. Electrochem. Soc.* **2019**, *166*, H791–H794.
[36] H. J. Kim, K. Kaplan, P. Schindler, S. Xu, M. M. Winterkorn, D. Heinz, T. English, J. Provine, F. B. Prinz, T. Kenny, *Appl. Mater. Interfaces* **2019**, *11*, 9594–9599.
[37] C. Chen, Y. Kang, Z. Huo, Z. Zhu, W. Huang, H. L. Xin, J. D. Snyder, D. Li, J. A. Herron, M. Mavrikakis, M. Chi, K. More, Y. Li, N. M. Markovic, G. A. Somorjai, P. Yang, V. R. Stamenkovic, *Science* **2014**, *343*, 1339–1343.
[38] H.-Y. Su, X.-H. Bao, W.-X. Li, *J. Chem. Phys.* **2008**, *128*, 194707.
[39] M. Nesselberger, M. Roefzaad, R. Fayçal Hamou, P. U. Biedermann, F. F. Schweinberger, S. Kunz, K. Schloegl, G. K. H. Wiberg, S. Ashton, U. Heiz, K. J. J. Mayrhofer, M. Arenz, *Nat. Mater.* **2013**, *12*, 919–924.
[40] S. Geiger, S. Cherevko, K. J. J. Mayrhofer, *Electrochim. Acta* **2015**, *179*, 24–31.
[41] J.-P. Grote, A. R. Zeradjanin, S. Cherevko, K. J. J. Mayrhofer, *Rev. Sci. Instrum.* **2014**, *85*, 104101.
[42] V. Komanicky, K. C. Chang, A. Menzel, N. M. Markovic, H. You, X. Wang, D. Myers, *J. Electrochem. Soc.* **2006**, *153*, B446–B451.
[43] U. Zerweck, C. Loppacher, T. Otto, S. Grafström, L. M. Eng, *Phys. Rev. B* **2005**, *71*, 125424.
[44] M. Rohwerder, F. Turcu, *Electrochim. Acta* **2007**, *53*, 290–299.
[45] A. A. Galuska, J. C. Uht, N. Marquez, *J. Vac. Sci. Technol. A: Vacuum, Surfaces, and Films* **1988**, *6*, 110.
[46] H. H. Hwu, J. G. Chen, *Chem. Rev.* **2005**, *105*, 185–212.
[47] M. Pourbaix, *Atlas of Electrochemical Equilibria in Aqueous Solutions*, NACE Interntional Ceelcor, Houston, Brussels, **1966**.
[48] R. D. Cowling, H. E. Hintermann, *J. Electrochem. Soc.* **1970**, *117*, 1447–1449.
[49] A. A. Topalov, I. Katsounaros, M. Auinger, S. Cherevko, J. C. Meier, S. O. Klemm, K. J. J. Mayrhofer, *Angew. Chem. Int. Ed.* **2012**, *51*, 12613–12615; *Angew. Chem.* **2012**, *124*, 12782–12785.
[50] S. T. Hunt, Y. Román-Leshkov, *Acc. Chem. Res.* **2018**, *51*, 1054–1062.

Manuscript received: February 19, 2020
Accepted manuscript online: March 12, 2020